A Polymer-Brush Templated Three-Dimensional Molybdenum Sulfide Catalyst for Hydrogen Evolution

Lucas-Alexandre Stern,[†] Piotr Mocny,[§] Heron Vrubel,[†] Tugba Bilgic,[§] Harm-Anton Klok[§,] and Xile Hu[†,*]*

† Laboratory of Inorganic Synthesis and Catalysis, Institute of Chemical Sciences and Engineering, École Polytechnique Fédérale de Lausanne (EPFL), ISIC-LSCI, BCH 3305, 1015 Lausanne (Switzerland), E-mail: xile.hu@epfl.ch

§ École Polytechnique Fédérale de Lausanne (EPFL), Institut des Matériaux and Institut des Sciences et Ingénierie Chimiques, Laboratoire des Polymères, Bâtiment MXD, Station 12, CH-1015 Lausanne (Switzerland), E-mail : harm-anton.klok@epfl.ch

KEYWORDS: hydrogen evolution, molybdenum sulfide, polymer brushes, electrocatalysis, atom transfer radical polymerization, X-ray photoelectron spectroscopy

ABSTRACT

Earth-abundant hydrogen evolution catalysts are essential for high-efficiency solar-driven water splitting. Although a significant amount of studies have been dedicated to the development of new catalytic materials, the microscopic assembly of these materials has not been widely investigated. Here we describe an approach to control the 3-dimensional (3D) assembly of amorphous molybdenum sulfide using polymer brushes as a template. To this end, poly(dimethylaminoethyl methacrylate) brushes were grown from highly-oriented pyrolytic graphite (HOPG). These cationic polymer films bind anionic MoS_4^{2-} through an anion exchange reaction. In a final oxidation step, the polymer-bound MoS_4^{2-} is converted into the amorphous MoS_x catalyst. The flexibility of the assembly design allowed systematic optimization of the 3D catalyst. The best system exhibited turnover frequencies up to 1.3 and 4.9 s^{-1} at overpotentials of 200 and 250 mV, respectively. This turnover frequency stands out among various molybdenum sulfide catalysts. The work demonstrates a novel strategy to control the assembly of HER catalysts.

INTRODUCTION

Hydrogen is considered to be the energy carrier of the future.[1] One of the most promising techniques for sustainable hydrogen production is water splitting. Water splitting consists of two half reactions, namely the hydrogen evolution reaction (HER) and the oxygen evolution reaction (OER). Electrocatalysts are employed to minimize the overpotential required to drive these reactions. Noble-metal electrocatalysts, notably Pt and its alloys, exhibit the highest reported activity for HER. However, due to the scarcity and high cost of Pt, large-scale implementation of water electrolyzers employing this material is not feasible. The development of Earth-abundant electrocatalysts for HER has become an active area of energy research. While many new classes of catalysts with promising activities, such as metal chalcogenides, phosphides, carbides, borides, nitrides have been reported,[2-5] much less attention has been paid to the microscopic assembly of the catalysts. Typically, the catalysts are simply casted from their suspensions onto supporting electrodes. Potential issues from this method include, but are not limited to, aggregation of nanoparticles and inhibition of individual active sites, low bulk conductivity, and hindered mass transport. Because a significant current density is required to produce a sufficient amount of hydrogen in HER, any practical device will consist of a catalyst layer of substantial thickness. Thus, the optimization of the 3D assembly of HER catalysts becomes important.[6]

MoS_x-polymer composites have previously been utilized for a number of applications.[7-10] The incorporation of MoS_2 within a polymer matrix has resulted in improved thermal, mechanical, and tribological properties of the materials.[11-12] Addition of MoS_2 to conductive polymers such as polypyrrole, polyaniline, poly(3,4-ethylenedioxythiophene leads to better supercapacitors.[13] Because MoS_x has been reported as an archetypical non-precious HER catalyst,[14-16], MoS_x-

polymer hybrids have also been evaluated for HER.[17-19] However, the performances of these composites is still modest.

Herein, we describe an approach to use polymer brushes as a template to control the 3D assembly of amorphous MoS_x. Polymer brushes are thin (typically 10 -200 nm thick) films consisting of chain end-surface tethered polymers. Polymer brush films are most frequently prepared by surface-initiated controlled radical polymerization chemistries, which allow precise control over polymer molecular weight (film thickness) and interchain distance (grafting density). As they can be prepared with precise control over film thickness, grafting density and can incorporate a range of chemical functional groups, polymer brush films are attractive templates for the templated formation of thin metal and metal oxide (composite) films.[20-23]In this report, we explore the use of polymer brushes to prepare a series of MoS_x-polymer composites on highly oriented pyrolytic graphite (HOPG) with variable heights, grafting densities, and site densities, which allowed a systematic study of parameters influencing the HER activity. HOPG is based on carbon which is abundant, and it is highly conductive and has a relatively flat surface. Thus, HOPG is preferred over silicon, which is highly resistive, and gold, which is rare and expensive. In terms of turnover frequency (TOF), a fundamental parameter in catalysis, our best catalyst is superior to most previously reported nanostructured molybdenum sulfide catalysts, with turnover frequencies of 1.3 and 4.9 s^{-1} at overpotentials of 200 mV and 250 mV, respectively. The study also reveals some of the challenges in this approach.

EXPERIMENTAL

Synthesis of (4-Nitrophenyl)diazonium tetrafluoroborate (4-NDT)

The diazonium salt was prepared in accordance with previous literature protocol.[24] A solution of 25 mmol $NaNO_2$ in 4 mL water was cooled down in an ice bath. 25 mmol of the corresponding aniline, in this case 4-nitroaniline (3.4 g), was added to 10 mL water. 9 mL HBF_4 was added to the aniline mixture and stirred vigorously. The reaction mixture turned brown after addition of the acid. The mixture was kept in an ice bath and left stirring for 5 to 10 minutes. Then the previously prepared sodium nitrite solution was added dropwise to the reaction mixture. Fumes were emitted upon the addition and the reaction mixture turned from brown to a mocha colour. The solution was left for 15 minutes. Meanwhile, some HBF_4 is cooled down in the meantime. Then, the reaction mixture was filtered. The filtered product was washed sequentially with the filtrate, the cold HBF_4 solution, ethanol and diethyl ether. The resulting (4-nitrophenyl)diazonium tetrafluoroborate was obtained as a khaki coloured paste. The reaction yield was 29% (1.1 g). The product was collected using a plastic spatula to reduce potential explosive hazards from diazonium compounds. 1H NMR (D2O, 400 MHz): δ (ppm) 8.95-8.92 (m, 2H), 8.79-8.76 (m, 2H).

Electrografting of the diazonium salt onto HOPG support

The details of the electrolyte bath composition are given in previous literature reports.[25] The grafting solution consisted in 0.1 M of NBu_4BF_4 and about 5 mM of diazonium salt in 30 mL acetonitrile (ACN). Depending on the grafting density desired, the 4-NDT and benzenediazonium tetrafluoroborate (BDT) concentrations were varied. A grafting density of 100% required 5 mM of 4-NDT, while 50% grafting density required 2.5 mM of BDT and 2.5 mM of 4-NDT in ACN. A grafting density of 10% required 4.5 mM of BDT and 0.5 mM of 4-NDT in ACN. The potentiostatic deposition was performed at a potential of -0.7 V vs. Ag/AgCl for 6 minutes. Each HOPG sample was carefully washed with water and acetone after grafting

and dried with nitrogen gas. After each grafting, the electrolyte was renewed and both the counter and the reference electrode were carefully rinsed with acetone and dried under nitrogen.

Preparation of poly(2-(methacryloyloxy)ethyl ammonium iodide) (PMETAI) brushes

Poly(2-(dimethylamino)ethyl methacrylate) (PDMAEMA) brushes were prepared according to a previous literature procedure.[22] Briefly, 15 mmol of DMAEMA (2.528 mL, 2.3583 g) and 0.3 mmol of the 2,2'-bipyridine ligand (0.0468 g) were mixed in deionized water (15 mL) and the mixture subjected to three consecutive freeze-pump-thaw cycles. Copper bromide (0.0215 g, 0.15 mmol) was then added under nitrogen atmosphere. Subsequent degassing by two additional cycles of freeze-pump-thaw was performed. All remaining solid was dissolved by continuous stirring at room temperature for 15 minutes. The mixture was then cannula transferred into a nitrogen-purged reaction vessel containing an HOPG plate with the attached ATRP initiator (for multiple surface grafting, the plates were mounted onto a custom made PEEK holders). The reaction was allowed to proceed at room temperature. The polymerization time was varied in order to evaluate the influence of the molecular weight of the polymer brush films on HER catalysis. On ZYA grade HOPG, polymerization times of 1, 5, 20, 40 and 60 minutes were used. Once the brushes were prepared, the HOPG plates were washed successively for 5 min with water, methanol and ethanol under nitrogen atmosphere. The prepared samples were then immersed in a 0.1 M solution of ethylenediaminetetraacetic acid (EDTA, adjusted to pH 8 with sodium hydroxide) for 1 hour. Final steps prior to quaternization included washing using water and ethanol and drying the samples in a stream of nitrogen. The resulting PDMAEMA brushes were placed within a PEEK holder into a glass reactor. The reactor was evacuated and backfilled with nitrogen 3 times. The samples were then quaternized using a 10 vol.% solution of methyl

iodide in acetone for 16 hours. The resulting PMETAI brushes were rinsed twice with each of the following solvent: acetone, ethanol, water and then again with ethanol. The quaternized brushes were then dried using nitrogen.

HER precatalyst incorporation

The iodide counter-anion was replaced by dipping the PMETAI-brush coated HOPG into a 40 mM solution of $(NH_4)_2MoS_4$ in dry dimethylformamide (DMF). Prior to submersion of the HOPG plates, the dipping mixture was stirred for 1 hour. Then, the mixture was filtered using a HPLC-syringe-filter made of a Nylon membrane with a pore size of 0.2 μm. The HOPG plates were placed separately in different vials. The filtrate was added to each vial and the HOPG plates were left submersed for one hour. Then, the plates were removed from the solution and washed carefully with water and acetone and dried under nitrogen. The as-prepared samples contained MoS_4^{2-}, which had replaced the iodide anions.

Physical characterization

XPS measurements were performed at the Molecular and Hybrid Materials Characterization Centre at the École Polytechnique Fédérale de Lausanne. The instrument used for surface analysis of the HOPG ZYH electrodes was an Axis Ultra instrument from Kratos Analytical equipped with a conventional hemispheric analyzer. The X-ray source employed was a monochromatic Al K_α source (1486.7 eV) source operating at 100 W and 10^{-9} mbar. The instrument used for HOPG ZYA plates surface analysis was a PHI5000 VersaProbe II XPS system by Physical Electronics (PHI) with a detection limit of 1 atomic percent. Analysis was performed using a monochromatic Al K_α X-ray source (1486.7 eV) of 24.8 W power with a

beam size of 100 µm. The spherical capacitor analyser was set at 45° take-off angle with respect to the sample surface. The pass energy was 46.95 eV yielding a full width at half maximum of 0.91 eV for the Ag 3d 5/2 peak. Curve fitting was performed using the PHI Multipak software. For survey analysis the pass energy was 187.8 eV with 0.8 eV/step. For multiplex analysis the pass energy was 46.9 eV with 0.2 eV/step or 23.9 eV with 0.1 eV/step. The diameter of the analysed area was 10 µm.

FTIR experiments were performed on a Vertex 80 from Bruker. The resolution was of 0.2 cm^{-1}. The infrared spectra were recorded on a 4000-400 cm^{-1} window using the attenuated total reflectance (ATR) mode. A platinum ATR crystal was used. The scan velocity was 10 kHz. A KBr beamsplitter was used.

Electrochemical measurements

Electrochemical measurements were recorded using a Gamry Instruments Reference 3000™ potentiostat. A traditional three-electrode configuration was used. For polarization and electrolysis measurements, a platinum wire was used as the counter electrode and a double-junction Ag/AgCl (KCl saturated) electrode was used as the reference electrode. Both the counter and reference electrode were rinsed with distilled water and dried with compressed air prior to measurements. The processed HOPG (home-made electrodes or plates) was used as working electrode unless stated otherwise. Potentials were referenced to a reversible hydrogen electrode by adding a value of (0.2 + 0.059×pH) V. All potentials were converted and referred to the RHE unless stated otherwise. The current density was normalised over the geometric surface area of the electrode. The value j_u, used to obtain a dimensionless logarithm, corresponds to a

unit current density of 1 A cm^{-2}. The ohmic drop was corrected using the current interrupt method.

RESULTS AND DISCUSSION

Figure 1 summarizes the synthetic strategy for the preparation of the MoS_x-polymer composites. First, (4-nitrophenyl)diazonium tetrafluoroborate was used to electrograft nitrobenzene onto the HOPG surface (Fig. 1, step 1). [25,26] Electrochemical reduction of the nitro group resulted in surface-bound aniline (Fig. 1, step 2). Reaction of this amino-functionalized surface with 2-bromo-2-methylpropionyl bromide (BiBB) (Fig. 1, step 3) followed by CuBr-catalyzed surface-initiated atom transfer radical polymerization (SI-ATRP) of dimethylaminoethyl methacrylate (DMAEMA) yielded a surface-attached polymer brush film (Fig. 1, step 4). The as-obtained PDMAEMA brushes were subsequently quaternized by methyl iodide to afford cationic PMETAI brushes (Fig. 1, step 5). This reaction was carried out using a previously reported procedure, which has been shown to result in quantitative conversion of the tertiary amine groups.[22] Ion exchange of the iodide anion in PMETAI with MoS_4^{2-} (Fig. 1, step 6), followed by oxidation resulted in an assembly containing MoS_3 as HER precatalyst.[15,27] The latter was converted to the active MoS_x catalyst during HER,[27,28] typically through 10 cathodic polarization scans. Detailed procedures for each of the steps in Figure 1 are provided in the Experimental Part and the Supporting Information.

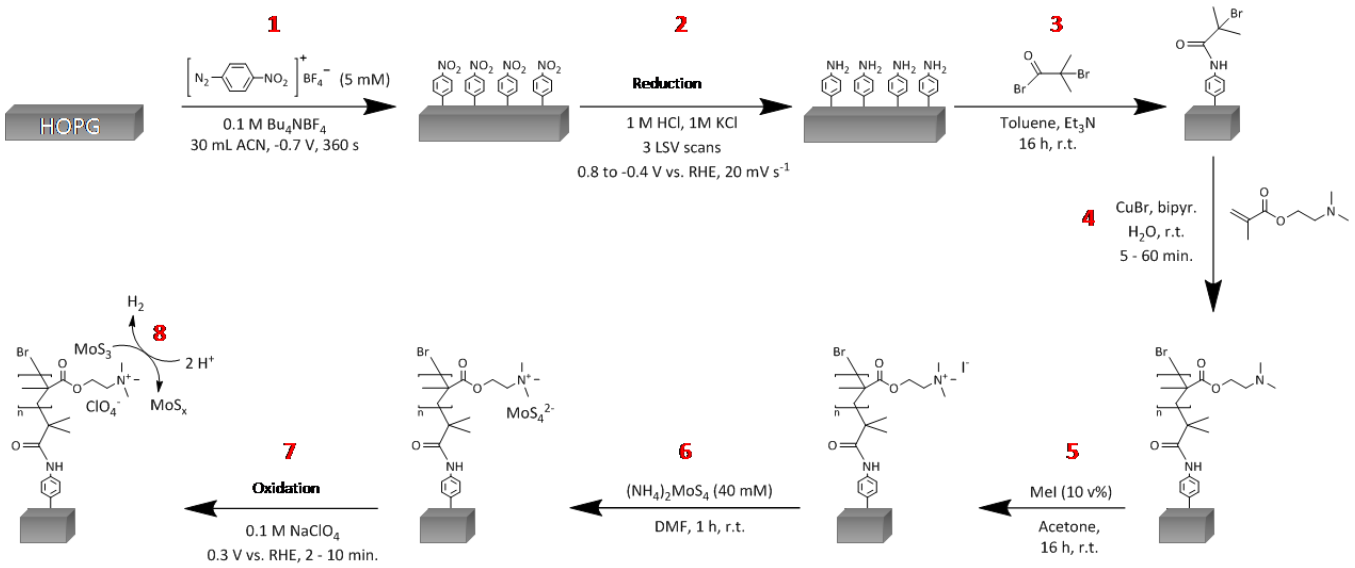

Figure 1. Synthetic procedure for the preparation of the MoS_x-polymer brush assemblies. A number is associated to each step of the process. For clarity, the number of anchoring molecules is reduced from four to one after step 3; (1) electrografting of nitrobenzene, (2) reduction of the nitro-anchored groups, (3) attachment of the ATRP initiator, (4) polymer brush growth, (5) quaternization of the polymer brushes, (6) catalyst incorporation via anion-exchange, (7) precatalyst formation, (8) HER catalysis.

Several HOPGs of different grades were used for the assembly. First HOPG ZYH plates were used (Fig. S1). X-ray photoelectron spectroscopy (XPS) measurements (Fig. S2) confirmed the formation of the desired assemblies. The wetting properties of the substrate at different stages of fabrication were evaluated using water contact-angle measurements (Fig. S3). The catalytic performance of the systems using HOPG ZYH substrates is summarized in Table S1. The performance of the reference sample prepared using Pt as catalyst indicates that the polymer network is not limiting the conductivity of the catalytic system for HER, probably because of the limited height of the polymer. The data in Table S1 indicate poor reproducibility of these systems, as significant variance in activity was observed on similar samples. We suspect that the

varying surface roughness of the HOPG ZYH substrates (Fig. S4) is the origin of this non-reproducibility. To mitigate this problem, the highest commercial grade of HOPG, *i.e.*, ZYA, was then employed as support. ZYH and ZYA HOPG bear a similar chemical composition, however, their mosaic spread, a measure of the parallelism of the crystalline grains in the materials, is different. ZYA has a lower mosaic spread (0.4°) than ZYH (3.5°),[29] and thus, has a significantly smoother surface. The ZYA samples are essentially flat on the nanometer level (Fig. S5).

AFM was used to monitor the evolution of the film thickness of PMETAI brushes grafted from HOPG ZYA and PDMAEMA brushes grafted from Si as a function of polymerization time. PDMAEMA brush films grafted from on Si samples were used as reference because the polymer heights could be reliably measured by ellipsometry. On the other hand, although HOPG is flat at a nanoscale, pronounced surface roughness can be observed at a micrometer scale (Fig. S6a), making the measurements of polymer heights by AFM less accurate. Despite the uncertainty, there is a visible correlation between polymerization time and brush film thickness for experiments on both HOPG plates and Si wafers (Fig. S6b). It was therefore possible to tune the length of the grafted polymer chains by varying time in the range of 5 to 60 minutes. We chose 20 minutes as an optimal polymerization time. On Si wafer the polymer growth started to slow down after 20 min, while on HOPG ZYA longer polymerization time seemed to lead to uncontrolled side reactions and non-reproducible polymer heights. Thus, for the following experiments the maximum polymerization time was set to 20 minutes.

To verify successful preparation of MoS_x-polymer assemblies, characterization of the samples at different stages of the assembly was performed. Fig. 2 shows Fourier-transform infrared (FTIR) spectra recorded at different stages of the fabrication process. Upon electrografting using

(4-nitrophenyl)diazonium tetrafluoroborate, absorption peaks of the nitro groups were observed at 1523 cm^{-1} and 1350 cm^{-1} in the infrared spectra (Fig. 2, red line).[30] The bands at 1590 cm^{-1} and 890 cm^{-1} were attributed to the HOPG support.[30] After the growth of the polymer brush film (Fig. 2, blue curve), the IR spectra of the samples were significantly modified and characteristic features of the PDMAEMA were revealed. Notably, the peak at 1730 cm^{-1} and the doublet observed at 1155 cm^{-1} were attributed to the C=O and C-O-C moieties, respectively.[31,32] The tertiary amine feature was present at 1400 cm^{-1}.[31] The signals attributed to the alkane moieties (CH_3, CH_2) of the brushes were found at 2950 cm^{-1} and 1475 cm^{-1}.[31,32] After anion-exchange (Fig. 2, green line), a new signal at 490 cm^{-1} is observed and is attributed to the Mo-S bond stretching vibration.[33] The HER catalysis converts the precatalyst MoS_3, to MoS_x. This conversion was reflected by the observation of new IR signals. The broad peak at 1650 cm^{-1} was attributed to MoS_x.[34] The slight shift of this peak compared to that of MoS_2 at 1630 cm^{-1} is consistent with the amorphous nature of our MoS_x catalyst (Fig. 2, orange curve). Overall the FTIR spectra indicate the successful preparation of the MoS_x-polymer composites.

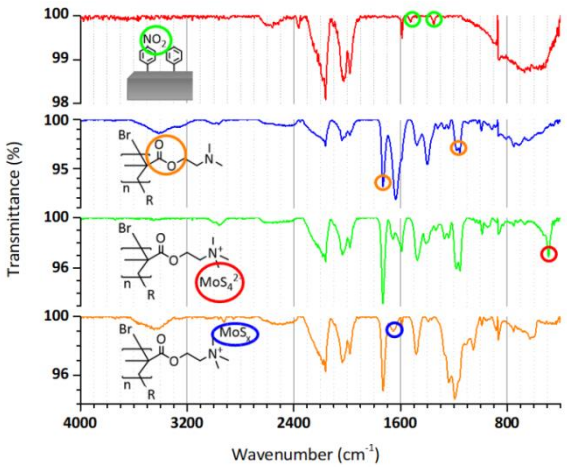

Figure 2. FTIR spectra of the MoS_x/polymer brush composite at different stages of fabrication. The corresponding chemical structure is drawn for reference. The circled features on the spectra

refer to the circled chemical moiety on the corresponding chemical structure. The "R" on the chemical structures is used to designate the covalent link between the polymer brush and the HOPG substrate, fabricated by the electrografting species and the ATRP initiator attachment. The features from 1900 to 2300 cm^{-1} are attributed to the oxidation of the support material, water and CO_2 traces.[35]

The successful preparation of the polymer composite films was also confirmed by XPS measurements, which were carried out at the different steps in the fabrication process (Fig. S7). N 1s high resolution XPS spectra were obtained for the first stages of brush-assembly preparation (Fig. 1, step 1-4). The main binding energies feature observed successively at 406. 1 eV (Fig. S7b), 399.7 eV (Fig. S7e), 399.9 eV (Fig. S7h), and 399.8 eV (Fig. S7l), correspond respectively to the nitro, amino, amide, and tertiary amine moieties. The presence of these specific features indicates the successful fabrication of the brush-assembly. Characteristic C 1s signals of PDMAEMA were also observed (Fig. S7m). The binding energies at 289.3, 286.9, and 285.3 eV, correspond respectively to the C-C=O, C=O, and C-O-C=O moieties of PDMAEMA. The O 1s features observed at 533.5 and 531 eV correspond to the O-C=O and O-C signals of the PDMAEMA brush (Fig. S7n). Deconvolution analysis of the XPS survey, high resolution spectra, and additional discussion is provided in the ESI. Fig. 3a and b show Mo 3d and S 2p deconvoluted XPS signals of the composite after catalyst incorporation (Fig. 1, step 6), while Fig. 3c and d present results for a composite sample after HER catalysis. After incorporation of the catalyst, the XPS signals indicate the presence of MoS_4^{2-} (230.9 eV), MoO_3 (232.8 eV), and molybdenum oxysulfide (231.8 eV).[27] The latter two are surface-bound impurities formed when the samples were exposed to air prior to XPS analysis; they are not expected to be present under catalytic conditions. For the catalyst after HER catalysis, the expected bridging S_2^{2-} and the

terminal S^{2-} associated with MoS_x are observed.[27] In addition, the S 2p XPS spectra reveals signals attributed to H_2S and H_2SO_4.[36-38] H_2SO_4 originates from the electrolyte. It has been reported that ammonium tetrathiomolybdate can generate H_2S under mild conditions.[39] The H_2S might remain in the composite, either being adsorbed by the polymer, or being dissolved in the electrolyte and trapped by the polymer. In addition, in-situ generation of H_2S via decomposition of the sample in the XPS experiments is possible.

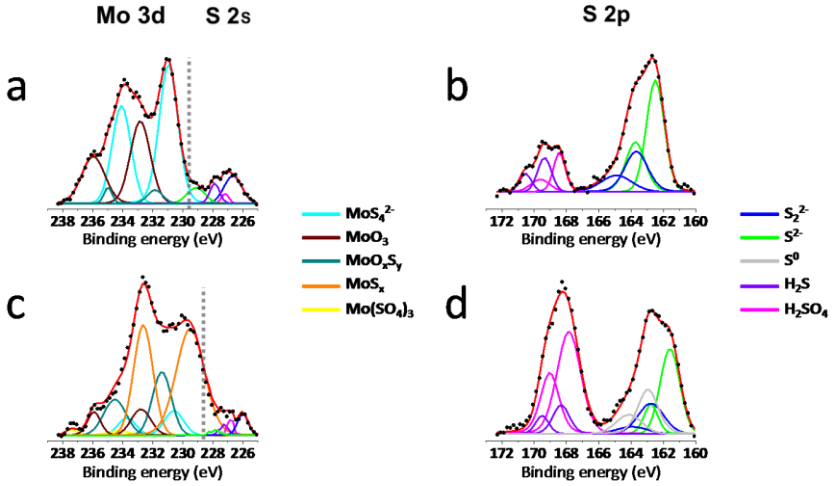

Figure 3. (a - c) Mo 3d high resolution XPS spectra for the composite sample after (a) catalyst incorporation and after (c) hydrogen evolution reaction. (b - d) S 2p high resolution XPS spectra for the composite sample after (b) catalyst incorporation and after (d) HER. The deconvolution follows a simple color code: the experimental data correspond to the black dots, the fitting envelope is the red line. Each coloured curve corresponds to a specific chemical moiety. Due to the degeneracy nature of the orbitals in S 2p and Mo 3d, each moiety possesses a doublet of signals. S 2s singlets are within the binding energy window of Mo 3d (right-hand side of the grey dashed line). The S 2s peak was deconvoluted using a curve for each moiety identified in the S 2p peaks deconvolution.

TEM images and corresponding elemental mapping information confirmed the successful incorporation of the catalyst after step 7 (Fig. 4). Focused-ion beam (FIB) was necessary to prepare the samples for imaging. The sample preparation process included the deposition of an amorphous carbon layer, to protect the composite from the milling step of the FIB process. To ensure a clear distinction from the carbon substrate and the protective carbon layer, a longer polymerization time, 40 minutes, was employed for the sample fabrication. Fig. 4a shows the cross-section TEM image of the sample, where the zones of HOPG, polymer layer, and protective carbon layer are visible. A higher resolution image is shown in Fig. 4b,. The corresponding elemental mapping images (Fig. 4c and d) confirm the presence of molybdenum sulfide within the polymer network. As expected, C signals have a lower intensity in the polymer layer than in the HOPG substrate and the protective carbon layer. Molybdenum is homogeneously distributed in the polymer layer.

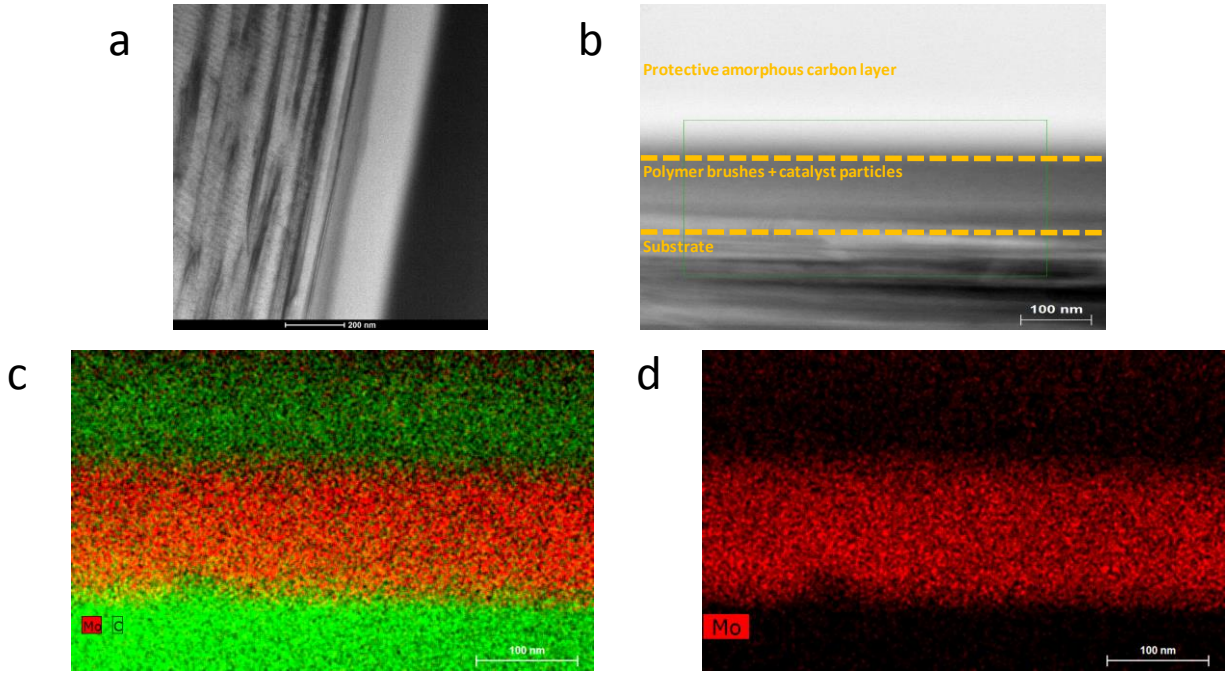

Figure 4. TEM and EDX images of the MoS_x-polymer composite on HOPG ZYA. The sample was prepared using focused-ion beam (FIB) to obtain a thin lamella sample that is measurable under TEM. (a) Overall cross section picture of the assembly (scale bar 200 nm). (b) Cross section image which served for EDX elemental mapping measurements. The dashed lines separate different regions of the sample. From bottom to top: substrate (HOPG) layer; polymer brushes with homogeneous incorporation of MoS_x; protective amorphous carbon layer (c) C and Mo elemental mapping. The brushes are sandwiched between the two carbon layers. (d) Mo elemental mapping. The polymer height is about *ca*. 150 nm.

The hydrogen evolving properties of the MoS_x-polymer composite films were tested using linear sweep voltammetry (LSV) in 1 M H_2SO_4. The samples were carefully insulated so that only a specific surface area of one HOPG face was exposed to the acidic media (Fig. S8). Fig. 5 shows representative LSV curves of the MoS_x-polymer composites made with polymerization time of 1, 5, and 20 minutes. The samples prepared with 20 minutes of polymerization time exhibited the highest net activity. An overpotential of 344 mV was required to generate a current density of 0.5 mA cm^{-2}. The relatively small current density achieved by the catalytic systems is largely due to a very small catalyst loading (Table S2). The intrinsic activity of the catalyst, however, can be described by turnover frequency (TOF). The loadings of MoS_x in these systems were measured using electrochemistry (ESI). Based on these data, the TOF at η = 250 mV was calculated (Fig 2, inset). It is noted that the TOFs of these composites are quite high, and are one order of magnitude higher than a previously reported MoS_x-polymer composite system.[19]

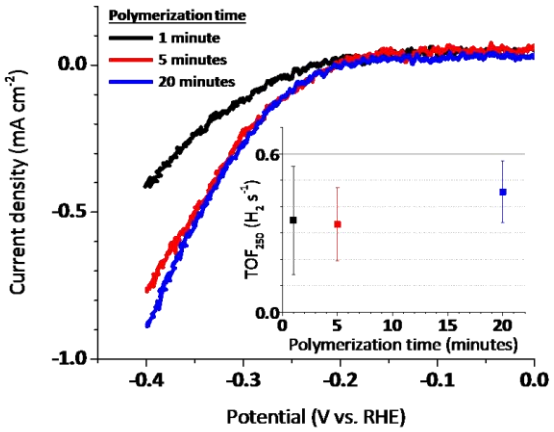

Figure 5. LSV scans (of MoS_x-loaded polymer brush films prepared using different polymerization times,. The assemblies underwent 10 consecutive LSV scans from 0.1 V to -0.4 V vs. RHE in 1 M H_2SO_4 to convert the precatalyst MoS_3 to the catalytic active species MoS_x. The scans displayed correspond to the 11th LSV measurement performed on the assemblies. Conditions: scan rate 5 mV s^{-1}, IR drop corrected. The catalyst loading for the polymer assemblies prepared at 1, 5, and 20 minutes polymerization times were 0.10, 0.18, and 0.17 µg cm^{-2}, respectively. Inset: turnover frequencies at η = 250 mV.

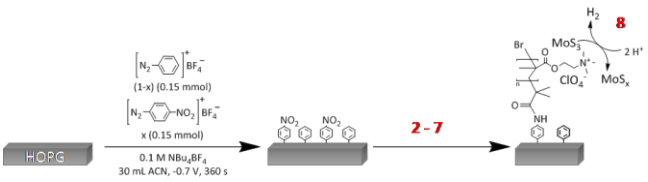

Figure 6. Schematic drawing of the method to vary the grafting density on HOPG. Parts 2-8 are identical to the steps described in Fig. 1.

Tafel analysis was conducted for the LSV curves of the assemblies (Table S2). The Tafel slopes are much higher than those of amorphous MoS_x[27,40-43], which suggests hindered electron and/or proton transport. The latter might originate from the hydrophobic nature of the polymer brushes. Water contact-angle measurements on the composites at several fabrication stages

support this hypothesis (Fig. S9). The bare HOPG substrate possesses a water-contact angle of 88.3°, indicative of a hydrophobic surface. Upon quaternization of the polymer brushes, a water-contact angle of 19.7° is observed (Fig. S9c). The surface prior to catalyst incorporation is thus hydrophilic. However, after catalyst incorporation and subsequent activation, the resulting assembly has a water-contact angle of above 95°, indicative of a very hydrophobic surface.

In the preparation of the above assemblies, HOPG was electrografted with nitrobenzene in a presumed 100% site density. As a consequence, the polymer brushes have a 100% grafting density. To probe the influence of the grafting density, polymer brushes with 50% and 10% grafting densities were also prepared. These samples were obtained by the introduction of non-polymerization active ("dummy") sites, i.e., benzene groups in the initial electrografting step. The benzene groups cannot be functionalized by the ATRP precursor, preventing the growth of polymer brushes from these sites. (Fig. 6). When polymer brush films are grown at identical polymerization times (~ molecular weights), the lower surface concentration of polymerization initiators on the 10% and 50% grafting density surfaces leads to an increased average interchain distance and thus a more collapsed polymer chain conformation and small film thickness.[20] Fig. 7 compares the LSV curves of three MoS_x-polymer assemblies, all made in 20 minutes but with different grafting densities. Table S3 and Fig. S10 describe further electrocatalytic data of additional samples. The overpotential required to generate a current density of 0.5 mA cm^{-2} for the composites prepared at 100%, 50%, and 10% grafting densities are 344, 254, and 211 mV, respectively. Thus, the catalytic performance is significantly improved upon reduction of the grafting density. Several factors contribute to the higher activity at reduced grafting density: (1) a higher catalyst loading (Table S3); (2) higher intrinsic activity (TOF) due to more accessible active sites (see below). (3) Additionally, mass transport might be more facile on samples with a

lower grafting density. The stability of the best catalyst was tested in a potentiostatic electrolysis for 10 hours. After an activation period (about 1 h), the current density remained largely stable (Fig. 7b). This result indicates a good stability of the activity of our catalyst.

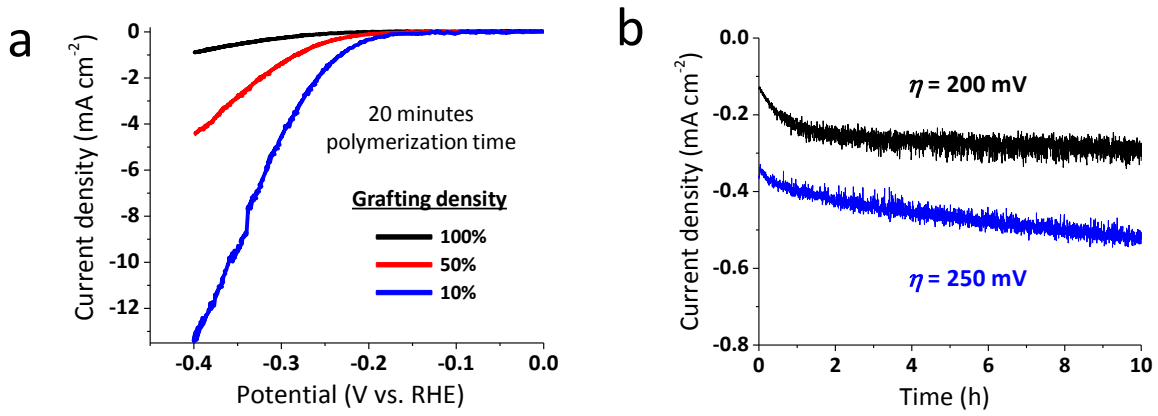

Figure 7. (a) LSV scans of MoS_x-coated polymer brush assemblies, prepared using 20 minutes of polymerization time and different grafting densities, in 1 M H_2SO_4. The assemblies underwent 10 consecutive LSV scans from 0.1 V to -0.4 V vs. RHE in 1 M H_2SO_4 to convert the precatalyst MoS_3 to the catalytic active species MoS_x. The scans displayed correspond to the 11th LSV measurement performed on the assemblies. Conditions: scan rate 1 mV s^{-1}, IR drop corrected. The catalyst loadings for the polymer assemblies prepared at 100%, 50%, and 10% grafting density were respectively 0.17, 0.12, and 0.35 µg cm^{-2}. (b) Potentiostatic electrolysis over 10 hours. The tested sample (catalyst loading of 0.35 µg cm^{-2}) was prepared under 10% grafting density and 20 minutes of polymerization time.

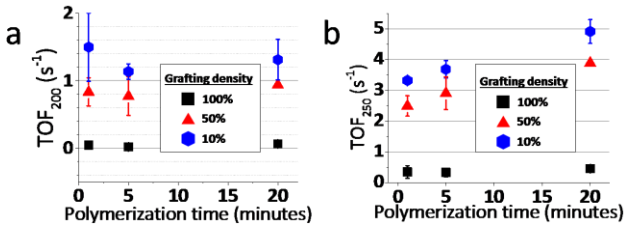

Figure 8. TOFs of the MoS_x polymer brush composites at different polymerization times and grafting densities. (a) TOFs at η = 200 mV; (b) TOFs at η = 250 mV. The averaged values of 3-4 samples in the same batch are displayed; error bars refer to standard deviation.

Fig. 8 shows the TOFs at η = 200 and 250 mV for the various samples prepared in this study. The figure shows that grafting density has a strong influence in TOF, while polymerization time (.i.e. polymer chain length) has only a modest influence. Despite different catalytic loadings (Table S3) of the samples prepared with identical polymerization time and grafting density, the activity in terms of TOF is similar. The most active catalyst is the sample with 10% grafting density and generated by 20 minutes polymerization of DMAEMA. TOFs of 1.3 and 4.9 s^{-1} at η = 200 and 250 mV were obtained. Fig. S11 shows that the activity of this catalyst is much higher than the catalyst directly deposited on HOPG. As mentioned above, the higher TOFs for the samples with lower grafting densities might be due to more accessible reaction sites. This may be due to the reduced steric hindrance as well as the smaller film thicknesses of the polymer composite films prepared from the lower grafting densities brushes.

The TOF values of the different catalysts are compared to some state-of-the-art molybdenum sulfide catalysts (Fig. 9).[19,27,44-48] Additional catalytic parameters including mass and specific activity, as well as TOFs, of the different catalytic systems are compared in Tables S4-S5.

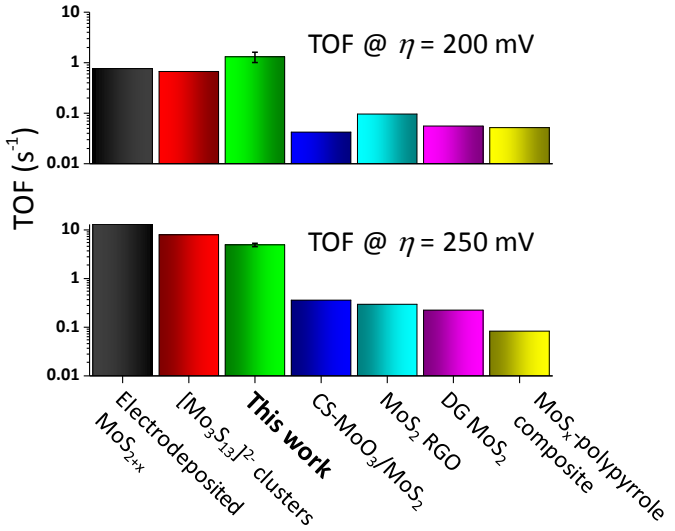

Figure 9. Comparison of TOFs of various state-f-the-art molybdenum sulphide catalysts. The electrodeposited MoS_{2+x} catalyst was previously developed by our group.[15] Jaramillo et al. developed the tetrathiomolybdate clusters $[Mo_3S_{13}]^{2-}$,[44] the core-shell MoO_3/MoS_2 nanowires,[45] and the double gyroid (DG) MoS_2 catalysts.[46] The MoS_2 RGO corresponds to molybdenum sulfide nanoparticles grown on reduced graphene oxide sheets suspended in solution.[47] The MoS_x polypyrrole composite correspond to electrodeposited molybdenum sulfide onto a poly(pyrrole-alkylammonium) matrix.[19]

It can be seen that the best MoS_x-polymer brush composite has higher TOFs than many MoS_2 nanoparticle catalysts. Its TOF is similar to that of $[Mo_3S_{13}]^{2-}$ clusters absorbed on HOPG which are rich in active edge sites, suggesting an optimal 3D assembly. Interestingly, the electrodeposited MoS_{2+x} film has also the highest activity among all these molybdenum sulfide catalysts, which serves as a fortuitous example of optimal random assembly.

Despite their high TOFs, the MoS_x-polymer brush composites have modest current densities at low overpotentials, which is due to low catalyst loadings. The maximum loadings of the catalyst

in the polymer brushes (it is assumed that the molecular weight (Mw) of MoS_x catalyst is similar to MoS_2, i.e. 160.1 g/mol) can be estimated according to this formula: mass loading = $Mw(MoS_2)*hd/(2M_{METAI})*$ where h is dry PMETAI brush thickness, d is polymer density of 1g/cm^3, and M_{METAI} = 299.1 g/mol. Thus, the maximum loadings are 1.04 μg cm^{-2} for 5 min polymerization time (assuming 38.8 nm brush height) and 2.14 μg cm^{-2} for 20 min polymerization time (assuming 80 nm brush height). Nevertheless, the measured actual catalyst loadings are typically lower and for highest film thicknesses they are as low as 10% of maximum values. We hypothesize that the entry of the catalyst in the polymer brush film is hindered due to the sterics of the polymer chains. This steric hindrance is reduced upon decreasing both film thickness and the grafting density, although the maximum loading is decreased as well.

CONCLUSIONS

In summary, a multiple-step synthetic protocol to prepare polymer brush-templated amorphous molybdenum sulfide catalysts has been successfully developed. The polymer brushes direct the 3D assembly of the MoS_x catalyst. Systematic investigations have led to an optimal catalyst template which is prepared by 20 minutes of polymerization of DMAEMA from ZYA HOPG substrate with 10% grafting density of the ATRP initiator. This catalyst shows turnover frequencies of 1.3 and 4.9 s^{-1} at η = 200 and 250 mV in 1 M H_2SO_4, which is among the highest reported for molybdenum sulfide catalysts. On the other hand, the geometrically averaged current densities at low overpotentials are comparatively small due to a very small loading of catalysts. How to significantly increase the catalyst loading in this system is the next challenge.

The work demonstrates a novel approach for the 3D assembly of HER catalysts, revealing its advantages and current limitation.

ASSOCIATED CONTENT

Supporting Information.

The supporting information is available free of charge.

Additional experimental methods and supplemental data (PDF)

AUTHOR INFORMATION

Corresponding Authors

*E-mail: xile.hu@epfl.ch

*E-mail: harm-anton.klok@epfl.ch

Author Contributions

The manuscript was written through contributions of all authors. All authors have given approval to the final version of the manuscript.

Funding Sources

This work is supported by a starting grant from the European Research Council (no 257096) to X.L. H.. H.-A. K. and P. M. acknowledge financial support from the Swiss National Science Foundation.

Notes

The authors declare no competing financial interest.

ACKNOWLEDGMENT

This work is supported by a starting grant from the European Research Council (no 257096) to X.L.H. H.-A. K. and P. M. acknowledge financial support from the Swiss National Science Foundation. We thank Barbora Bartova and Dr. Duncan Alexander of the Interdisciplinary Centre for Electron Microscopy of EPFL for FIB sample preparation, TEM, and EDS measurements, and Laurent Liardet (EPFL) for potentiostatic electrolysis experiments. We thank Prune Hu (Suricate Design) for help with the Table of Content graphic.

REFERENCES

(1) Anderson, D.; Holdren, J. P.; Jefferson, M.; Jochem, W.; Nakićenović, N.; Reddy, A. K. N.; Rogner, H.-H.; Smith, K. R.; Turkenburg, W. C.; Williams, R. H. *World Energy Assessment*, United Nations Development Programme, New York, 2000.

(2) Zou, X.; Zhang, Y. Noble Metal-Free Hydrogen Evolution Catalysts for Water Splitting *Chem. Soc. Rev*., **2015**, 44, 5148-5180.

(3) Roger, I.; Shipman, M. A.; Symes, M. D. Earth-Abundant Catalysts for Electrochemical and Photoelectrochemical Water Splitting *Nat. Rev. Chem.*, **2017**, 1, 0003.

(4) Jiao, Y.; Zheng, Y.; Jaroniec, M.; Qiao, S. Z. Design of Electrocatalysts for Oxygen- and Hydrogen-Involving Energy Conversion Reactions *Chem. Soc. Rev.*, **2015**, 44, 2060–2086.

(5) Faber, M. S.; Jin, S.; Earth-Abundant Inorganic Electrocatalysts and Their Nanostructures for Energy Conversion Applications *Energy Environ. Sci.* **2014**, 7, 3519–3542.

(6) Zhao, H.; Zhu, Y.-P.; Yuan, Z.-Y. Three-Dimensional Electrocatalysts for Sustainable Water Splitting Reactions *Eur. J. of Inorg. Chem.,* **2016**, 13-14, 1916-1923.

(7) Coleman, J. N.; Lotya, M.; O'Neill, A.; Bergin, S. D.; King, P. J.; Khan, U; Young, K; Gaucher, A; De, S; Smith, RJ; Shvets, I.V.; Arora, S.K.; Stanton, G; Kim, H.Y.; Lee, K.; Kim, G.T.; Duesberg, G.S.; Hallam, T; Boland, J.J.; Wang, J.J.; Donegan, J.F.; Grunlan, J.C.; Moriarty, G.; Shmeliov, A.; Nicholls, R.J.; Perkins, J.M.; Grieveson, E.M.; Theuwissen, K.; McComb, D.W.; Nellist, P.D.; Nicolosi, V. Two-dimensional nanosheets produced by liquid exfoliation of layered materials. *Science*, **2011**, 331, 568-571.

(8) Rao, C. N. R.; Ramakrishna Matte, H. S. S.; Maitra, U. Graphene analogues of inorganic layered materials. *Angew. Chem. Int. Ed.*, **2013**, 52, 13162-13185.

(9) Zhou, K.; Liu, J., Zeng; W., Hu; Y.; Gui, Z. In situ synthesis, morphology, and fundamental properties of polymer/MoS_2 nanocomposites. *Compos. Sci. Technol.*, **2015**, 107, 120-128.

(10) Wang, X.; Xing, W.; Feng, X.; Song, L.; Hu, Y. MoS_2/Polymer Nanocomposites: Preparation, Properties, and Applications. *Polym. Rev.*, **2017**, 57, 440-466.

(11) Naffakh, M.; Díez-Pascual, A. M.; Remškar, M.; Marco, C. New inorganic nanotube polymer nanocomposites: improved thermal, mechanical and tribological properties in isotactic polypropylene incorporating INT-MoS_2. *J. Mater. Chem.*, **2012**, 22, 17002-17010.

(12) Yuan, H.; Yang, S.R.; Liu, X.H.; Wang, Z.F.; Ma, L.M.; Hou, K.M.; Yang, Z.G.; Wang, J.Q. Polyimide-based lubricating coatings synergistically enhanced by MoS_2@ HCNF hybrid. *Composites: Part A*, **2017**, 102, 9-17.

(13) Zhang, W. J.; Huang, K. J. A review of recent progress in molybdenum disulfide-based supercapacitors and batteries. *Inorg. Chem. Front.*, **2017**, 4, 1602-1620.

(14) Laursen, A. B.; Kegnæs, S.; Dahl, S.; Chorkendorff, I. Molybdenum Sulfides—Efficient and Viable Materials for Electro- and Photoelectrocatalytic Hydrogen Evolution *Energy Environ. Sci.*, **2012**, 5, 5577–5591.

(15) Merki, D.; Hu, X. Recent Developments of Molybdenum and Tungsten Sulfides as Hydrogen Evolution Catalysts *Energy Environ. Sci.*, **2011**, 4, 3878–3888.

(16) Benck, J. D.; Hellstern, T. R.; Kibsgaard, J.; Chakthranont, P.; Jaramillo, T. F. Catalyzing the Hydrogen Evolution Reaction (HER) with Molybdenum Sulfide Nanomaterials *ACS Catal.*, **2014**, 4, 3957–3971

(17) Zeng, X.; Niu, L.; Song, L.; Wang, X.; Shi, X.; Yan, J. Effect of Polymer Addition on the Structure and Hydrogen Evolution Reaction Property of Nanoflower-Like Molybdenum Disulfide. *Metals*, **2015**, 5, 1829-1844.

(18) Dai, X.P.; Du, K.L.; Li, Z.Z.; Sun, H.; Yang, Y.; Zhang, X. ; Li, X.S.; Wang, H. Highly efficient hydrogen evolution catalysis by MoS 2–MoN/carbonitride composites derived from tetrathiomolybdate/polymer hybrids. *Chem. Eng. Sci.*, **2015**, 134, 572-580.

(19) Lattach, Y.; Deronzier, A.; Moutet, J. C. Electrocatalytic Hydrogen Evolution from Molybdenum Sulfide-Polymer Composite Films on Carbon Electrode *ACS Appl. Mater. Interfaces*, **2015**, 7, 15866–15875.

(20) Zoppe, J. O.; Ataman, N. C.; Mocny, P.; Wang, J.; Moraes, J.; Klok, H.-A. Surface-initiated controlled radical polymerization: state-of-the-art, opportunities and challenges in surface and interface engineering with polymer brushes, *Chem. Rev.* **2017**, *117*, 1105 – 1318.

(21) Tugulu, S.; Harms, M.; Fricke, M.; Volkmer, D.; Klok, H.-A. Polymer brushes as ionotropic matrices for the directed fabrication of microstructured calcite thin films, *Angew. Chem.* **2006**, *118*, 7619 – 7623; *Angew. Chem. Int. Ed.* **2006**, *45*, 7458 – 7461.

(22) Paripovic, D.; Klok, H.-A. Polymer Brush Guided Formation of Thin Gold and Palladium/Gold Bimetallic Films *ACS Appl. Mater. Interfaces*, **2011**, 3, 910–917.

(23) Sugnaux, C.; Mallorquí, A. D.; Herriman, J.; Klok, H.-A.; i Morral, A. F. Polymer brush guided formation of conformal, plasmonic nanoparticle-based electrodes for microwire solar cells, *Adv. Funct. Mater.* **2015**, *25*, 3958 – 3965.

(24) Starkey, E. B. *p*-Dinitrobenzene *Org. Synth.*, **1939**, 19, 40.

(25) Delamar, M.; Hitmi, R.; Pinson, J.; Saveant, J. M. Covalent Modification of Carbon Surfaces by Grafting of Functionalized Aryl Radicals Produced from Electrochemical Reduction of Diazonium Salts *J. Am. Chem. Soc.*, **1992**, 114, 5883–5884.

(26) Allongue, P.; Delamar, M.; Desbat, B.; Fagebaume, O.; Hitmi, R.; Pinson, J.; Savéant, J. M. Covalent Modification of Carbon Surfaces by Aryl Radicals Generated from the Electrochemical Reduction of Diazonium Salts *J. Am. Chem. Soc.*, **1997**, 119, 201–207.

(27) Vrubel, H.; Hu, X. Growth and Activation of an Amorphous Molybdenum Sulfide Hydrogen Evolving Catalyst *ACS Catal.*, **2013**, 3, 2002–2011.

(28) Lassalle-Kaiser, B.; Merki, D.; Vrubel, H.; Gul, S.; Yachandra, V. K.; Hu, X.; Yano, J. Evidence from in Situ X-ray Absorption Spectroscopy for the Involvement of Terminal Disulfide in the Reduction of Protons by an Amorphous Molybdenum Sulfide Electrocatalyst *J. Am. Chem. Soc.*, **2015**, 137, 314–321.

(29) Patel, A. N.; Collignon, M. G.; O'Connell, M. A.; Hung, W. O.; McKelvey, K.; Macpherson, J. V.; Unwin, P. R. A new view of electrochemistry at highly oriented pyrolytic graphite. *J. Am. Chem. Soc.*, **2012**, 134, 20117-20130.

(30) Leitner, T.; Kattner, J.; Hoffmann, H. Infrared Reflection Spectroscopy of Thin Films on Highly Oriented Pyrolytic Graphite *Appl. Spectrosc.*, **2003**, 57, 1502–1509.

(31) Zhang, X.; Li, G.; Zhang, H.; Wang, X.; Qu, J.; Liu, P.; Wang, Y. Enhanced Adsorption Capacity and Selectivity towards Salicylic Acid in Water by a Cationic Polymer Functionalized 3-D Ordered Macroporous Adsorbent *Soft Matter*, **2013**, *9*, 6159–6166.

(32) Taktak, F.; Yildiz, M.; Sert, H.; Soykan, C. A Novel Triple-Responsive Hydrogels Based on 2-(Dimethylamino) Ethyl Methacrylate by Copolymerization With 2-(N-morpholino) Ethyl Methacrylate *J. Macromol. Sci. Part A*, **2015**, 52, 39–46.

(33) Zhang, J.; Hu, S. P.; Feng, Y. L.; Xu, B.; Guo, Y. H. Synthesis and Characterization of Rodlike Ammonium Tetrathiomolybdate and its Thermal Decomposition Mechanism *Adv. Mater. Res.*, **2011**, 287–290, 2049–2052.

(34) Maugé, F.; Lamotte, J.; Nesterenko, N. S.; Manoilova, O.; Tsyganenko, A. A. FT-IR study of surface properties of unsupported MoS_2 *Catal. Today*, **2001**, 70, 271–284.

(35) Socrates, G. *Infrared and Raman Characteristic Group Frequencies*, John Wiley & Sons, Ltd., Chichester, 2001.

(36) Sodhi, R. N.; Cavell, R. G. KLL auger and core level (1s and 2p) photoelectron shifts in a series of gaseous sulfur compounds *J. Electron Spectrosc. Relat. Phenom.*, **1986**, 41, 1–24.

(37) Benck, J. D.; Chen, Z. B.; Kuritzky, L. Y.; Forman, A. J.; Jaramillo, T. F. Amorphous Molybdenum Sulfide Catalysts for Electrochemical Hydrogen Production: Insights into the Origin of their Catalytic Activity *ACS Catal.*, **2012**, 2, 1916–1923.

(38) Weber, T.; Muijsers, J. C.; Niemantsverdriet, J. W. Structure of Amorphous MoS_3 *J. Phys. Chem.*, **1995**, 99, 9194–9200.

(39) Xu, S.; Yang, C. T.; Meng, F. H.; Pacheco, A.; Chen, L.; Xian, M. Ammonium Tetrathiomolybdate as a Water-Soluble and Slow-Release Hydrogen Sulfide Donor *Bioorg. Med. Chem. Lett.*, **2016**, 26, 1585–1588.

(40) Merki, D.; Fierro, S.; Vrubel, H.; Hu, X. Amorphous Molybdenum Sulfide Films as Catalysts for Electrochemical Hydrogen Production in Water *Chem. Sci.*, **2011**, 2, 1262–1267.

(41) Merki, D.; Vrubel, H.; Rovelli, L.; Fierro, S.; Hu, X. Fe, Co, and Ni Ions Promote the Catalytic Activity of Amorphous Molybdenum Sulfide Films for Hydrogen Evolution *Chem. Sci.*, **2012**, 3, 2515–2525.

(42) Vrubel, H.; Merki, D.; Hu, X. Hydrogen Evolution Catalyzed by MoS_3 and MoS_2 Particles *Energy Environ. Sci.*, **2012**, 5, 6136–6144.

(43) Vrubel, H.; Moehl, T.; Grätzel, M.; Hu, X. Revealing and Accelerating Slow Electron Transport in Amorphous Molybdenum Sulphide Particles for Hydrogen Evolution Reaction *Chem. Commun*., **2013**, 49, 8985-8987.

(44) Kibsgaard, J.; Jaramillo, T. F.; Besenbacher, F. Building an Appropriate Active-Site Motif into a Hydrogen-Evolution Catalyst with Zhiomolybdate $[Mo_3S_{13}]^{2-}$ Clusters *Nat. Chem.*, **2014**, 6, 248–253.

(45) Chen, Z.; Cummins, D.; Reinecke, B. N.; Clark, E.; Sunkara, M. K.; Jaramillo, T. F. Core–Shell MoO_3–MoS_2 Nanowires for Hydrogen Evolution: A Functional Design for Electrocatalytic Materials *Nano Lett.*, **2011**, 11, 4168–4175.

(46) Kibsgaard, J.; Chen, Z.; Reinecke, B. N.; Jaramillo, T. F. Engineering the surface structure of MoS_2 to preferentially expose active edge sites for electrocatalysis. *Nat. Mater.*, **2012**, 11, 963–969.

(47) Li, Y.; Wang, H.; Xie, L.; Liang, Y.; Hong, G.; Dai, H. MoS_2 Nanoparticles Grown on Graphene: An Advanced Catalyst for the Hydrogen Evolution Reaction *J. Am. Chem. Soc.*, **2011**, 133, 7296–7299.

(48) Li, D. J.; Maiti, U. N.; Lim, J.; Choi, D. S.; Lee, W. J.; Oh, Y.; Lee, G. Y.; Kim, S. O. Molybdenum Sulfide/N-Doped CNT Forest Hybrid Catalysts for High-Performance Hydrogen Evolution Reaction *Nano Lett*,. **2014**, 14, 1228−1233.

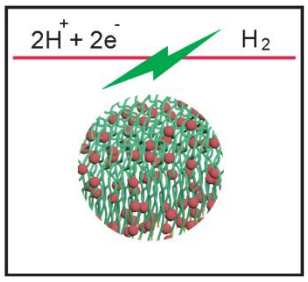
2H+ + 2e-
H2